



# The potential impacts of a water transfer project on the groundwater system in the Sugan Lake Basin of China

Zhengqiu Yang<sup>1,2,3</sup> · Litang Hu<sup>1,2,3</sup> · Kangning Sun<sup>1,2,3</sup>

Received: 15 June 2020 / Accepted: 15 March 2021 / Published online: 25 March 2021  
© Springer-Verlag GmbH Germany, part of Springer Nature 2021

## Abstract

The ungauged Sugan Lake Basin represents a candidate area for development of a water transfer scheme to satisfy the water requirement of Dunhuang city in northwestern China. In this work, multisource data, including river runoff, groundwater levels and remote-sensing data, and field investigation records, were collected and analyzed. A three-dimensional groundwater flow model was constructed using FEFLOW software to predict the potential influence of the transfer project on the groundwater system. Results show that infiltration from the Great Harten River is the main driving factor of groundwater-level fluctuation and groundwater recharge. Scenario analysis under four water transfer conditions found that the drawdown of groundwater gradually decreases from east to west. If the water transfer scale reaches  $1.2 \times 10^8 \text{ m}^3/\text{a}$ , after 100 years, the maximum drawdown of groundwater is noted at 68.02 m, and the flow rate of the Middle Spring reduces by 25.7%. In the western wetland, the area over which the groundwater level is lowered by more than 4 m is  $10.21 \text{ km}^2$ , and natural succession may occur or vegetation cover may decline. The results of this study will aid in water resource planning based on a rational amount of water transfer, and provide further protection of the wetland ecology.

**Keywords** Groundwater/surface-water relations · Interbasin water transfer · Numerical modeling · Arid regions · China

## Introduction

Arid and semiarid lands are distributed globally and carry 38% of the world's population (Huang et al. 2015; Reynolds et al. 2007). In these regions, water shortage problems are the major limitation of social and economic development (Feng et al. 2011; Mohammed and Scholz 2018; Scanlon et al. 2010; Luo et al. 2020). A well-functioning ecosystem, which is

sensitive to the quantity and quality of water resources, is essential to maintain cultivatable and habitable drylands (Hruska et al. 2017; Zhang et al. 2016; Zhou et al. 2016). However, it is challenging to maintain the balance between development and the environment by exclusively depending on the water resources of the dry basin itself. For instance, headwater damming leads to river cutoff, reduced groundwater levels in the downstream area, and even further ecological degradation or even destruction (Kingsford and Thomas 2004; Lin et al. 2018).

In this context, interbasin water transfer projects have been widely applied to alleviate water scarcity in many countries such as Canada (Deepak 2006), China (Liu and Zheng 2002), India (Bhaduri and Barbier 2011), Iran (Ahmadi et al. 2019), South Africa (Bourblanc and Blanchon 2014) and the United States (Rodrigues et al. 2014). These projects have caused significant impacts on the agriculture, environment, and wetland ecology of both water-receiving and water-supplying areas (Howe et al. 1990; Zhang et al. 2018; Zhou et al. 2016). Tien et al. (2020) evaluated the influence of surface waters of the Gadar basin (Iran) that were recharged by the water delivered from the Zab River (Iran). Zhu et al. (2018) assessed the decline in groundwater levels and the process of

✉ Litang Hu  
litanghu@bnu.edu.cn

Zhengqiu Yang  
zhengqiu\_y@mail.bnu.edu.cn

Kangning Sun  
201931470034@mail.bnu.edu.cn

- <sup>1</sup> College of Water Sciences, Beijing Normal University, Beijing 100875, China
- <sup>2</sup> Beijing Key Laboratory of Urban Hydrological Cycle and Sponge City Technology, Beijing 100875, China
- <sup>3</sup> Engineering Research Center of Groundwater Pollution Control and Remediation of Ministry of Education, Beijing 100875, China

vegetation succession in the Nalenggele River Basin, a donor basin in the dryland of northwest China. However, Gohari et al. (2013) used a system dynamics model to demonstrate that the water transfer plan in the Zayandeh-Rud River Basin (Iran) might have negative consequences due to an improper water policy. Deepak (2006) summarized Canada's diversion projects and argued that they bring substantial benefits as well as ecologically intricate impacts. Other studies show that extracting river flows not only reduces river stage but also affects groundwater levels (Rivière et al. 2014; Roy et al. 2015; Tian et al. 2015), which is a critical factor that influences ecological systems in arid regions in addition to climate changes (Jolly et al. 2008; Lyu et al. 2019).

Dunhuang city is located in the western section of the Hexi Corridor (China), one part of the Old Silk Road from the Han Dynasty. It is a tourist city with famous attractions such as the Crescent Lake, Mingsha Mountain, and Mogao Caves (Ma et al. 2013; Lin et al. 2018). Over recent decades, water resources have been overexploited to meet the demand of tourism due to the limited water resources (annual precipitation <45 mm) and intense human activities (Jiao 2010). As a result, the Chinese government initialized a project called "Comprehensive Planning for the Rational Utilization of Water Resources and Ecological Protection of Dunhuang" in 2009 to rationally utilize water resources and adequately protect the ecological environment in the Dunhuang area. The proposed key measures in this project include river dredging, control of groundwater use, water-saving projects, and an interbasin water transfer project. The Harten-Dang water diversion project is a fundamental measure, in which water from the Great Halten River (GHR) in the Sugan Lake Basin (SLB) will be transferred to the upstream area of the Dang River. The amount of water to be transferred remains unknown. The SLB, which is close to Dunhuang city and uninhabited, has relatively considerable water resources and two nature preservation zones. Both catchments are located in an arid region; however, the research on hydrogeology at SLB is lacking. Xiang et al. (2020) classified the hydrochemical characteristics of groundwater samples in the SLB and evaluated the water quality, but the study could not fully explain the origin of groundwater due to the lack of environmental isotopes sampling. The relationship among the rivers, groundwater, and lakes to support the balance between water diversion and wetland ecology are critical issues to be addressed (Vrzel and Vižintin Ogrinc 2019). The objectives of this study are (1) to form a comprehensive understanding of the hydrogeological condition of the SLB by analyzing data from multiple sources; (2) to simulate relationships between groundwater and surface water using numerical models; and (3) to assess the potential impacts on groundwater and wetland ecology induced by the Harten-Dang water transfer project. First, combined with observational data on groundwater levels, river runoff and remote-sensing images of GHR, the

relationship among the river, lakes, and groundwater were analyzed. Based on the aforementioned work, the conceptual model of the groundwater system was constructed. Then, a three-dimensional (3D) numerical groundwater model for SLB is established and calibrated using FEFLOW software. Under four scenarios, with  $0.6 \times 10^8$ ,  $0.8 \times 10^8$ ,  $1.0 \times 10^8$  and  $1.2 \times 10^8$  m<sup>3</sup>/a transfer scales, the calibrated model was applied to assess variations in water table and groundwater discharge. Finally, impacts on wetland ecology were predicted by the relationship between wetland vegetation and groundwater level, which is derived from field investigation.

## Materials and method

### Study area

The SLB is located on the northern edge of the Qinghai-Tibet plateau in northwest China (Fig. 1b). It extends from 93°40' to 95°30'E, 38°40' to 39°10'N, with an area of approximately 15,000 km<sup>2</sup>. The surrounding mountains, including Algin, Danghenan, Chaganebotu, Turgendaban, and Saishiteng mountains, are distributed modern glaciers with elevations greater than 4,800 m above sea level. The lowest elevation of the SLB is approximately 2,800 m. The typical arid plateau climate leads to freezing, windy, and dry weather. The yearly average temperature is between −5.6 and 3.7 °C, and the average daily temperature from November to March is below 0 °C. Figure 2b shows that both precipitation and potential evaporation are uneven in space and time (Gansu Institute of Geo-Environment Monitoring (GIG-EM), 'Investigation on groundwater circulation and water balance in the Sugan Lake Basin (in Chinese)', unpublished report, 2009). The average annual rainfall of the lake region is 18.8 mm, whereas this value can exceed 100 mm at the GHR gauge (Fig. 2a). In terms of temporal distribution, most rainfall occurs from May to September, accounting for more than 70% of the yearly precipitation (Fig. 2b). The potential evaporation is greater than 2,000 mm/a, and the amount of evaporation in summer is greater compared with other seasons. Therefore, rainfall outside the wetlands area does not directly recharge groundwater because of intense evaporation and a deep water table, and river leakage is the primary source of groundwater recharge (GIG-EM, 'Hydrogeological investigation and groundwater flow process analysis in the Sugan Lake Basin (in Chinese)', unpublished report, 2019).

The SLB is an endorheic basin. Two perennial rivers, the GHR and the Little Harten River (LHR), rise in the eastern mountains with average runoff of 300 and 66 million m<sup>3</sup>/a, respectively (GIG-EM, 'Special report on hydrology and water resources of water diversion project, Gansu province, China (in Chinese)', unpublished report, 2016). The rivers are fed by groundwater, glacial

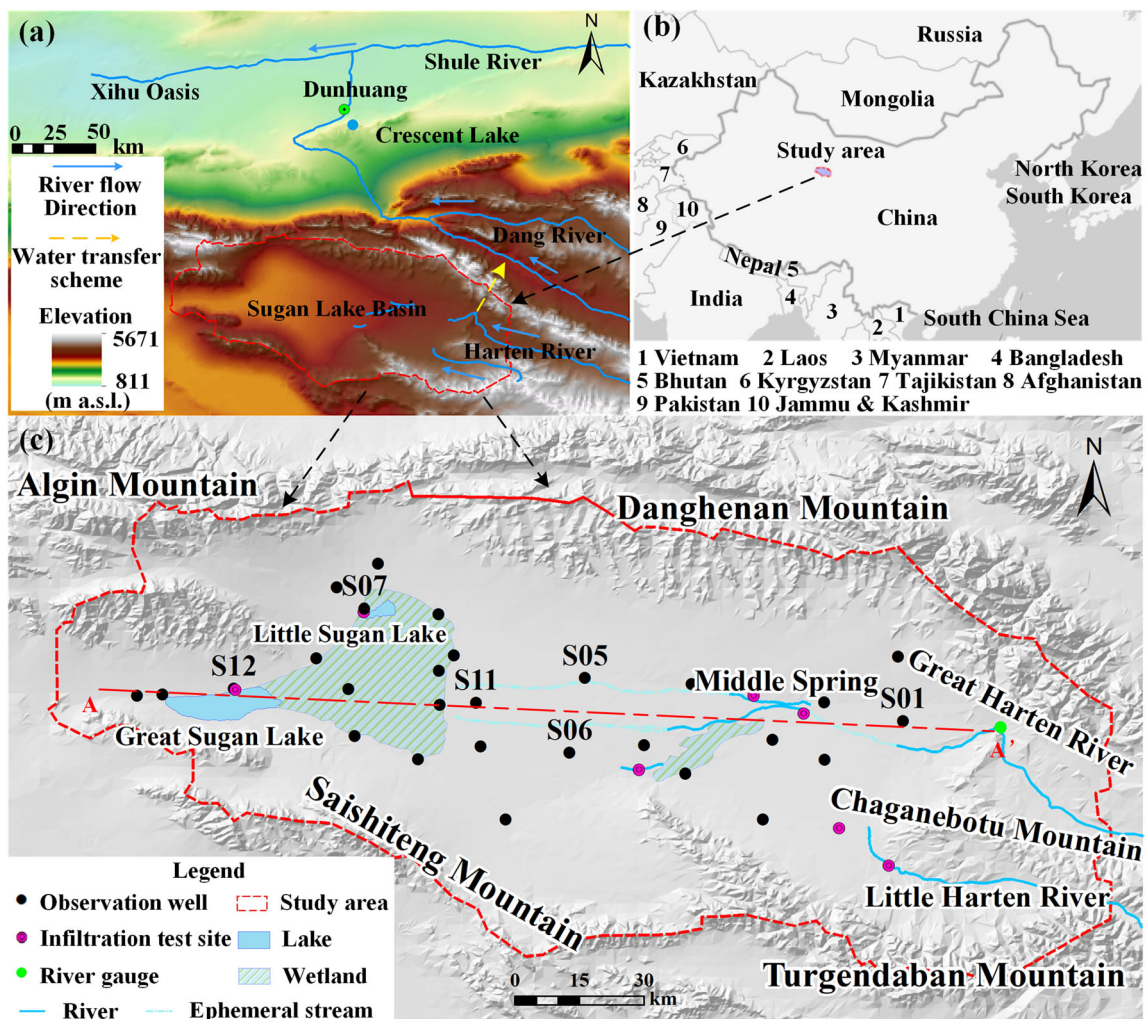
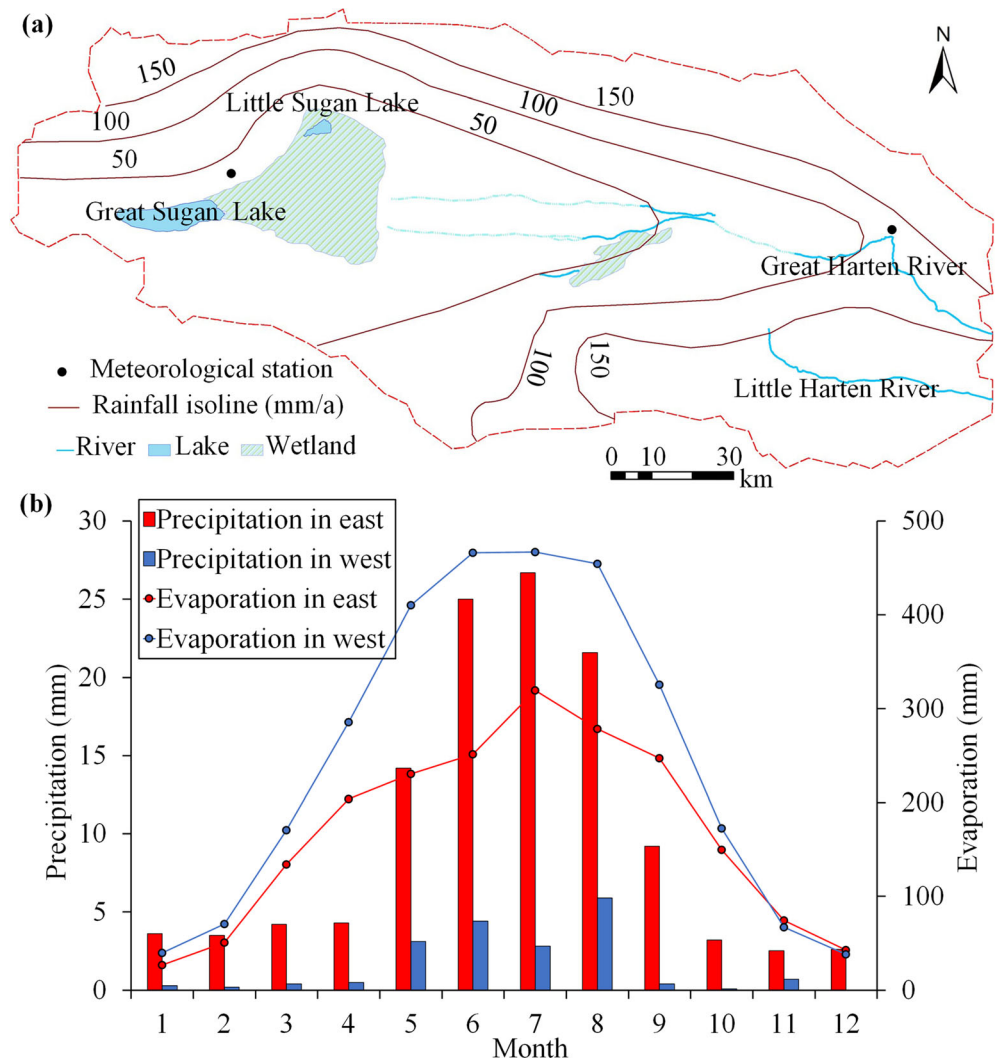


**Fig. 1** Map of the study area: **a** water systems and water transfer map of the Sagan Lake Basin and the Dang River Basin; **b** the location of the study area on a large scale; **c** the location of observation sites, surface-water network, wetlands, and the cross-section line of A–A'

meltwater and rainfall. Runoff series were collected from a river gauge (Fig. 1c). Under the driver of the topography terrain, the river and groundwater flow from west to east. However, the river course is discontinuous, and ephemeral streams exist during the rainy season from July to September (Fig. 1c). Groundwater drains into surface water due to the variation in topography and lithology in the Middle Spring (Fig. 3), and part of the spring water infiltrates back into the groundwater. Eventually, the groundwater sinks into lakes or evaporates from wetlands and returns to the atmosphere (GIG-EM, unpublished report, 2009, detailed previously). According to ICESat and ICESat2 (ICE, Cloud, and land Elevation Satellite) data, the water levels of Great Sagan Lake (GSL) and Little Sagan Lake (LSL) slightly fluctuated at elevations 2,793 and 2808 m, respectively. The areas of the GSL and the LSL measured by Google Earth images are approximately 106.0 and 10.6 km<sup>2</sup>, respectively.

As shown in Fig. 1c, the two wetlands are located around the Middle Spring and the two lakes respectively. The 2019 unpublished report by GIG-EM, detailed previously, describes the monitoring of flow of surface water in two wetlands throughout 2018, and revealed that the groundwater vastly discharges at the eastern edge of the western wetland. Then, the groundwater forms streams that flow through the western wetland into the GSL rather than directly discharge into the GSL (GIG-EM, unpublished report, 2019). Freeze-thaw water replenishes wetland groundwater in early March each year. At this time, the wetland groundwater level is the highest in the year. Wetlands also provide habitats for wild horses, camels, and 47 species of birds and other wild animals (Bao et al. 2007; Ma et al. 2015). The western wetland is a natural reserve protected by national environmental laws, covering an area of about 850 km<sup>2</sup>. Agriculture, animal husbandry, and tourism have been restricted, and human consumption of water resources is negligible.

**Fig. 2** Rainfall and evaporation of the Sugan Lake Basin (GIG-EM, unpublished report, 2019). **a** Annual average rainfall isoline map with meteorological station location; **b** the variation of average monthly rainfall and evaporation at two meteorological stations



**Hydrogeology**

The Sugan Lake depression is a secondary tectonic unit in the northern Qaidam uplift that was formed in the Late Cretaceous of Mesozoic (Fan et al. 2016). The exposed bedrock strata

include Proterozoic marble and gneiss; sandstone, limestone, and shale from the Paleozoic period; and Mesozoic mudstone and sandstone. The bedrock around the SLB forms boundaries separating other hydrogeological units. On the western side of the SLB, low ridgy terrain is present at the junction of the

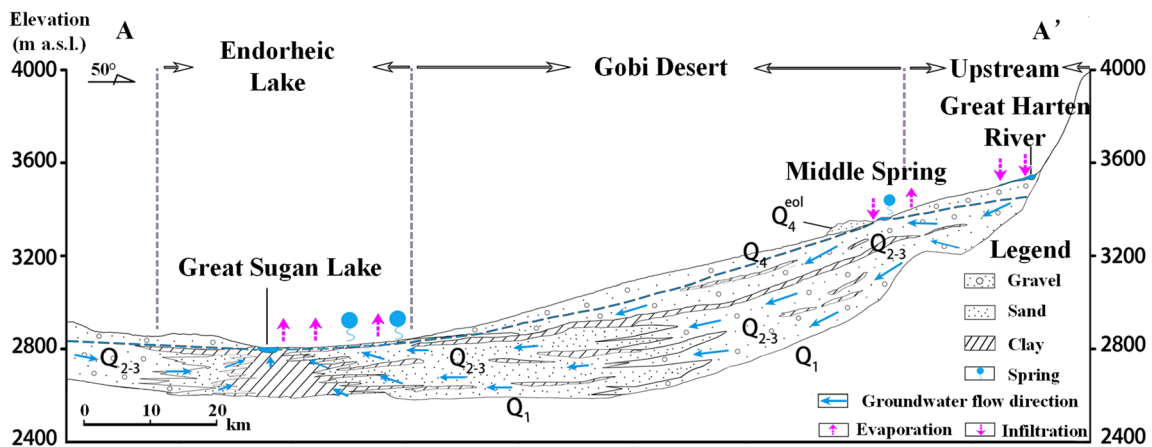


**Fig. 3** The hydrogeological cross-section extending along the groundwater flow direction of the Sugan Lake Basin

Algin and Saishiteng mountains, which serve as a barrier to lateral outflow. The Quaternary sediment outcrops are limnetic sandy-clay; glacial boulder-clay; alluvial pebble and sand-gravel; and aeolian sand. Quaternary strata are the principal aquifer medium in the SLB, with an exceptional thickness (GIG-EM, unpublished report, 2009). According to the lithology revealed by borehole logs (GIG-EM, unpublished report, 2016, detailed previously), the formations can be generalized into three layers vertically: the phreatic aquifer on the top, the middle aquitard, and the confined aquifer at the bottom. The phreatic aquifer lies in the Holocene ( $Q_4$ ) and the upper Pleistocene ( $Q_3$ ) strata (Fig. 3). The thickness of the phreatic layer ranges from 10 to 150 m. The second layer consists of glaciofluvial deposited clay at the top of the middle Pleistocene ( $Q_2$ ) with a thickness of 10–50 m. The confined aquifer is located in the stratum of  $Q_2$ . However, most drilled boreholes did not entirely penetrate the full aquifer, especially in the middle area of the basin (the thickness is greater than 200 m), so the confined aquifer is set above a supposed lower Pleistocene series ( $Q_1$ ), which is considered an impermeable layer.

The whole aquifer system of the SLB can be divided into three zones from the debouchure to inland lakes (Fig. 3), with the exception of the poorly permeable strata formed by glacial till in the foothills. In the upper stream, the aquifer consists of alluvium and aeolian deposits. The permeability from the top of the alluvial fan to the fine soil plain (the Middle Spring) gradually decreases. The lithology changes from pebbles to fine sand and sandy-clay. The aquifer in the Gobi region has good permeability and is composed of diluvial gravel and aeolian sandy deposits. Single-well pumping test results in the Gobi (Fig. 3) demonstrate that the hydraulic conductivity can exceed 45 m/day. In the lake zone, the aquifer is semipermeable and mainly composed of limnetic sediments. Double-ring infiltration test results reveal less than 1 m/day hydraulic conductivity.

### Remote-sensing images

Remote-sensing images supplement field surveys at high elevations, especially given the harsh environment—see the electronic supplementary materials (ESM). Landsat is a series of observation satellites managed by NASA (National Aeronautics and Space Administration) and USGS (United States Geological Survey) to explore the earth's resources and to monitor the environment. Data are available on the USGS website (USGS 2020). Landsat 5 and Landsat 8 data in the rainy season (July to September) from 2000 to 2018 were downloaded, and 18 scenes with the lowest cloud cover were selected to identify river morphology and wetland shape. Sensors carried by satellites generate multi-band data, and the red, green and blue bands were fused into true-color images. The surface-water network is identified by the visual

observation method from those images. The surface elevations of lakes were extracted from the GLA14 data (ICESat-1 level-2 product) from 2003 to 2009 and the ATL14 data (ICESat-2 level-3A product) from 2018 to 2019 (Jasinski et al. 2020).

### Numerical model

#### Conceptual model

The area of the model domain is approximately 15,000 km<sup>2</sup>. Model boundaries along mountain ridgelines were set as no-flow boundaries (Fig. 1c) because they are the borders that divide the groundwater systems of the SLB from other basins. Lateral flow comes from the eastern border, which is represented by the inflow boundary. The model structure can be generalized by three layers with two aquifers and one aquitard. The bottom of the model extends to the contact between the Quaternary deposits and bedrock as a no-flow boundary. The thickness of the phreatic and confined aquifer is 8–170 and 200 m, respectively. The aquitard lies in the middle with a width of 10 m. Partitioning of the hydraulic conductivity ( $K$ ), specific yield ( $S_y$ ) and storage coefficient ( $S_s$ ) is shown in Fig. 4 with a total of 27 zones based on a field survey (GIG-EM, unpublished report, 2009).  $K$  in each parameter zone is regarded as horizontally isotropic, while the vertical  $K$  is supposed to be equal to one-third of the horizontal  $K$ .

The interaction between groundwater and surface water is embodied in three processes in the model. First, rivers infiltrate the phreatic aquifer because river water stages in the upstream are higher than groundwater levels. Then, controlled by the geomorphologic and lithological change, the groundwater overflows the first time and forms the Middle Spring. However, the spring will seep back into the groundwater soon. Eventually, the groundwater will drain to the GSL, the LSL, and the surrounding wetland. The lakes zone is the lowest-lying area of the basin and the terminus of the groundwater system.

#### Numerical model setup

FEFLOW is a finite-element-based simulation software (Diersch 2014), which has advantages over the finite-difference method in model structure characterization. Triangularly meshed grids were refined in key research areas, including nearby springs, lakes, and rivers. Based on the conceptual model, a 3D groundwater model was established using FEFLOW. The whole area was divided into 29,616 elements (9,872 per layer) with 14,820 nodes (4,940 per layer). The simulation lasted 31 months from June 2016 to January 2019. Automatically controlled time

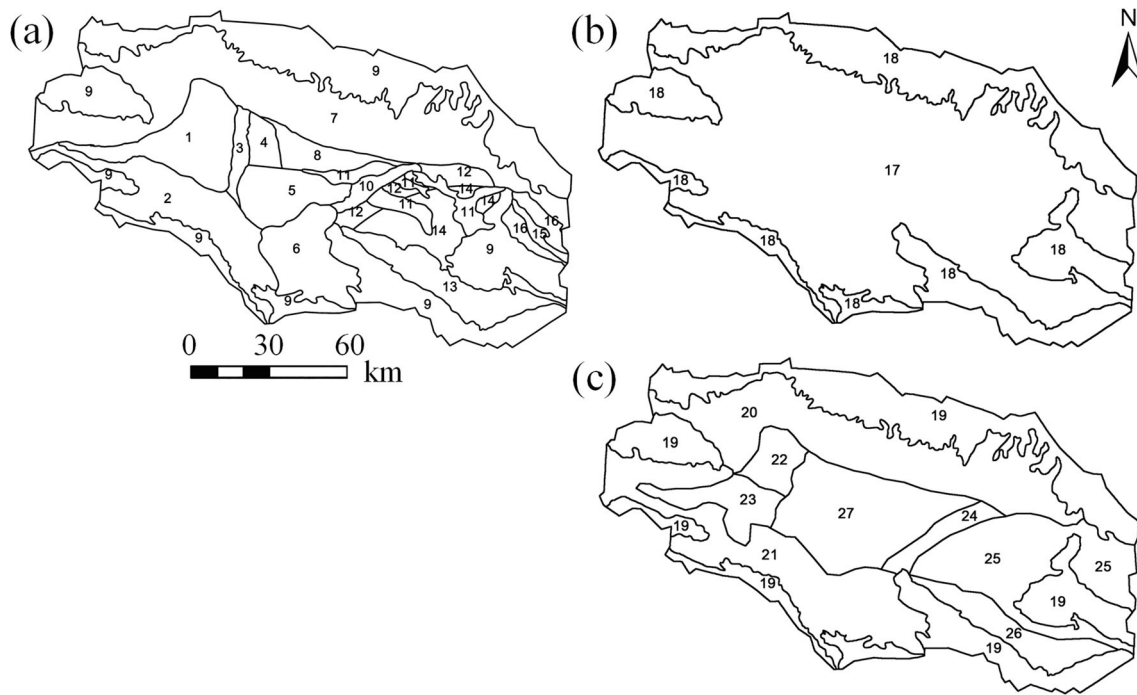


**Fig. 4** Hydrogeological parameter zonation: **a** phreatic aquifer, **b** aquitard and **c** confined aquifer

steps are applied in the model. DEM (digital elevation model) data were obtained from Google Earth and were used to interpolate surface elevation.

Precipitation infiltration is the product of the rainfall and infiltration coefficient, and the infiltration coefficients are related to the underlying surface and groundwater depth. Groundwater/surface-water interactions are not incorporated in the model, because it is difficult to simulate discontinuous surface water (ephemeral stream in Fig. 1c) using existing model functions such as the Cauchy boundary. Therefore, river and seasonal stream infiltration recharge groundwater in the form of 109 injection wells, while 30 wells of seasonal streams work only during wet seasons. The amount of river infiltration is equal to baseflow, and more water than the base flow in the wet season is injected into groundwater by 30 wells. Springs and wetlands are considered as drains that can be represented by the seepage surface function in FEFLOW. When the groundwater level of the seepage node is greater than the specified level during simulation, the groundwater drains until the water table is lower than this level. The return flow from the Middle Spring to groundwater is equal to the spring flow measured in the field (GIG-EM, unpublished report, 2019) and is set as the Neumann boundary. The lateral flow of the eastern mountain also is treated as the Neumann boundary in the model, and flux is calculated according to the hydraulic gradient of groundwater and hydraulic conductivity. Limited by the model function, the evaporation process is not set in the model, so it will be included in the discharge to the wetland. Lakes are set as fixed head boundaries in the model with a stable water level.

Manual trial-and-error adjustment and FePEST (automatic parameter estimation module in FEFLOW) (Doherty 2010) were both used in the study, and the parameter calibration process includes two steps. First, a steady flow model of SLB was established. The hydraulic conductivities of 27 parameter zones were optimized according to the initial distribution of water level interpolated from the borehole data of groundwater. Initial values of parameters were given based on results of single-well pumping tests and double-ring infiltration tests (Fig. 1c). Then, adjusted coefficients were applied to the transient model, and  $S_y$  and  $S_s$  were optimized with dynamic data using FePEST. The calibration period is from June 2016 to December 2017, while the validation period is from January 2018 to January 2019 with a total running time of 950 days. The determination coefficient ( $R^2$ ), mean absolute error (MAE), and root mean square error (RMSE) between simulated and observed groundwater levels in 28 observation wells (Fig. 1c) were used to evaluate validity (House et al. 2015).

#### Data sources

Table 1 shows the sources of data collected. Data on groundwater levels and spring flow were obtained from GIG-EM, which also provided pumping test reports for 15 boreholes. Precipitation data were obtained from local meteorological stations (Fig. 2a). The hydrological station of Halten River (Fig. 1c) provided information about river runoff, which is discontinuous before 2009. DEM data (30 m × 30 m resolution) were downloaded from Google Earth and interpolated

**Table 1** Sources of input data used in the model

Data type	Number	Time series	Time scale	Data source
Precipitation	43	2016–2019	Monthly	Meteorological stations
Groundwater level	441	2016/7–2019/1	Daily	GIG-EM
Elevation	N/A	N/A	N/A	Google Earth
Runoff	207	1956–2018	Monthly	Hydrological stations
Lake water level	N/A	N/A	Occasionally	ICESat and ICESat2
Spring flow	12	2018	Monthly	GIG-EM
Hydraulic conductivity	22	N/A	N/A	Double-loop test/ Pumping test reports

using the Kriging method. The water levels of lakes were observed using ICESat satellite data. These underlying data were further processed into acceptable monthly forms for the model or visualized as figures to analyze the results.

## Results

### Changes of groundwater level in recent years

Over past decades, the runoff of the GHR indicates an upward trend. The 10-year average flow rate increased from  $2.61 \times 10^8 \text{ m}^3/\text{a}$  (1990–1999) to  $3.48 \times 10^8 \text{ m}^3/\text{a}$  (2000–2009) and  $3.90 \times 10^8 \text{ m}^3/\text{a}$  (2009–2018). It peaked at  $4.56 \times 10^8 \text{ m}^3/\text{a}$  in 2018 (GIG-EM, unpublished report, 2019). A similar phenomenon was also found in some studies of northwest China (Hu and Jiao 2015; Li et al. 2012; Shi et al. 2006; Wang et al. 2018). As a result, the groundwater storage has also increased (Fig. 5, boreholes S01, S05, S06, S11). However, water table curves show different dynamic patterns. S01 is located in the upstream area (Fig. 1c), and the periodic variation in river leakage has strongly influenced groundwater levels, resulting in a fluctuating increase. There was a delay in peaks, which usually appeared in December rather than the rainy season due to the distance between S01 and the river, which is approximately 10 km. By contrast, given that S05 is close to the channel, the water level increase in S05 immediately occurred during the wet season when the aquifer accepted the leakage from ephemeral reaches. The water level of S05 increased by 14.79 m in 2018, and reached a peak elevation of 3,016.56 m. The northern basin received an enormous amount of recharge in 2018 given the northward movement of the watercourse. From July 2016 to December 2018, the water table of S06 and S11 increased at rates of 1.83 and 0.60 m/a, respectively. The observations of S06 and S11 in the Gobi zone show a pattern of steady increase. These two locations are far enough from rivers that the aquifer can dampen the fluctuation of recharge. The rise of the water table in S06 is more prominent since this borehole is located closer to the upstream than S11. The relation between the river and aquifer is the principal factor

affecting the water table, especially in the upstream and Gobi Desert.

### Model calibration and validation

After model calibration,  $R^2$ , MAE, and RMSE from the simulated results are listed (Table 2). For high-elevation regional models (Lin et al. 2018; Yao et al. 2015), these indices indicate that the model is well calibrated. Model errors during the verification period did not show an obvious accumulating trend (Fig. 5). The reason for the small error is that the conceptual and numerical models capture well the natural groundwater regime, which is relatively well-understood because the natural character of the basin is not disturbed by human activities. The maximum absolute error of all boreholes is 5.5 m, which occurred at the junction between bedrock and porous media in Danghenan Mountain, given that the terrain is steep.

Compared with S05, the  $R^2$  of S01 simulations is lower, indicating that the fitting of the groundwater regime is unsatisfactory. The lateral flow from the Danghenan Mountain was potentially underestimated, which leads to the lower simulation value. The determination coefficients of S06 and S11 illustrate that the model well fits water-table changes in the Gobi region (Table 2). S07 and S12 lie in the western part of the basin, where the water table is comparatively stable. The model has difficulty in simulating the dynamic change in S07 because this study did not consider the evaporation intensity change and freezing–thawing process in the wetland (Fig. 5, S07). S12 sits on the northern side of the lake zone, where groundwater is recharged by the lateral flow from the Algin Mountain. The groundwater level of S12 remained constant for years given the long distance between the source and sink and the deeper water level compared with the evaporation extinction depth.

### Groundwater flow and budgets

The hydraulic gradient of Gobi Desert is less than 3%, while that of some hillsides is greater than 10% (Fig. 6). The apparent differences in hydraulic gradients are controlled by the

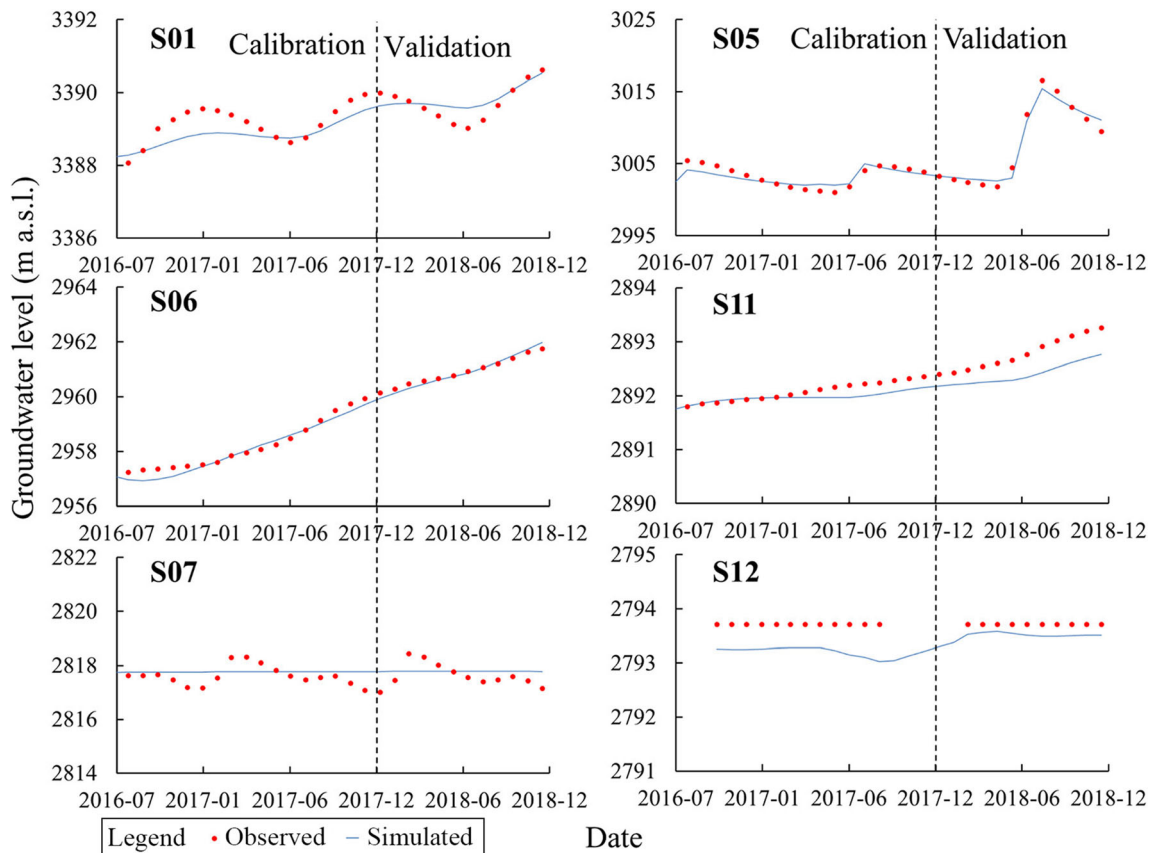


**Fig. 5** Comparison between observed and simulated values of six typical boreholes (locations shown in Fig. 1c)

slant of the confining bed and the permeability of water-bearing media. The maximum flow rate of groundwater can reach 0.22 m/day in the upstream zone. Groundwater flows are slowest in the lake zone, where the hydraulic gradient is less than 0.5% and the permeability is poor. The hydraulic gradient in the hillslope is the largest, but the flow velocity there is not fast given the low permeability of the moraine. Near the Middle Spring, groundwater drainage and reinfiltration caused the groundwater contour to bend (Fig.

6). Overall, the simulated groundwater field is reasonable, demonstrating the reliability of the model.

Four recharge items and two discharge items are present in the water budget table (Table 3). The discharge of groundwater to the Middle Spring and the recharge of return flow are internal terms and not listed in the table. Table 3 presents the water budget and summarizes the average of the simulation results of 2 years from 2017 to 2018 because the simulation duration of 2016 is only half a year. The recharge of river leakage is  $3.01 \times 10^8 \text{ m}^3/\text{a}$ , and that of the infiltration of the seasonal stream is  $1.88 \times 10^8 \text{ m}^3/\text{a}$ . The combined recharge of runoff is  $4.89 \times 10^8 \text{ m}^3/\text{a}$ , accounting for 90.56% of all replenishment. As mentioned previously, the river runoff has increased in recent years, so the total amount of river water is considerably increased in the simulation period compared with the average annual runoff from 1990 to 2018 ( $3.66 \times 10^8 \text{ m}^3/\text{a}$ ). The rainfall infiltration is  $0.43 \times 10^8 \text{ m}^3/\text{a}$ , and the recharge of lateral flow from the eastern side of the basin is  $0.08 \times 10^8 \text{ m}^3/\text{a}$ . For discharge items, the groundwater drainage to wetlands is  $4.22 \times 10^8 \text{ m}^3/\text{a}$ , while the discharge into lakes is quite small ( $0.21 \times 10^8 \text{ m}^3/\text{a}$ ). The result is consistent with the actual situation. Groundwater storage increases by an average of  $0.97 \times 10^8$  per annum, indicating that the recharge volume is much higher than discharge in 2017 and 2018.

**Table 2** Indexes of simulation results of calibration and validation period

Observation site	Calibration			Validation		
	RMSE	MAE	$R^2$	RMSE	MAE	$R^2$
S01	0.39	0.33	0.80	0.29	0.24	0.73
S05	1.27	1.05	0.81	1.34	1.10	0.97
S06	0.21	0.18	0.96	0.13	0.11	0.99
S07	0.39	0.33	0.01	0.40	0.35	0.81
S11	0.14	0.10	0.84	0.4	0.38	0.96
S12	0.50	0.49	0	0.21	0.19	0.10
All results	1.41	1.11	0.99	1.95	1.15	0.98



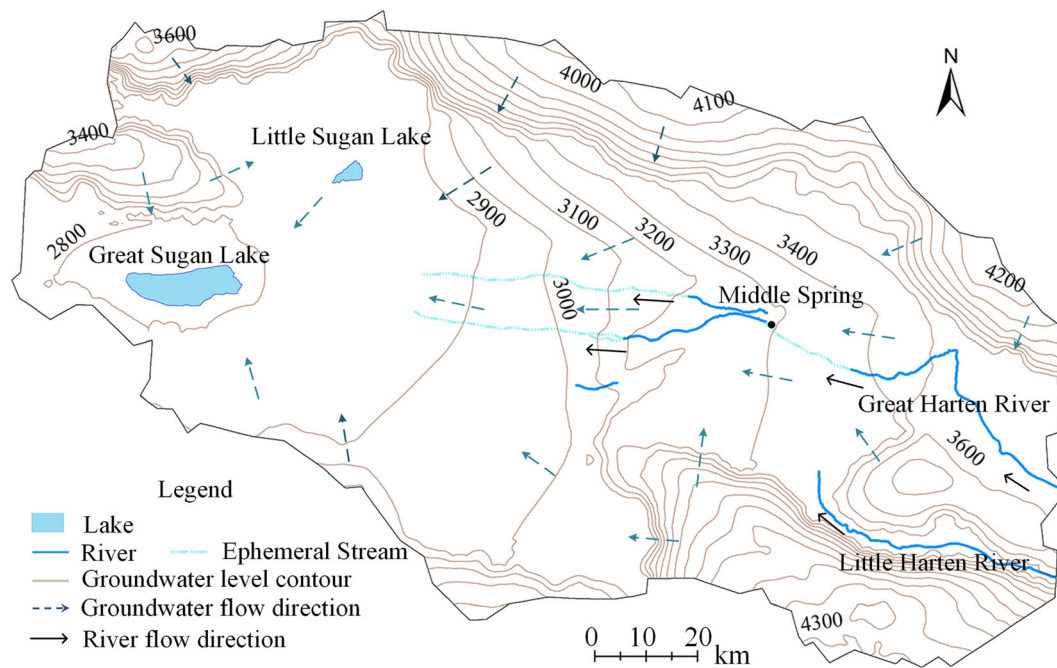


Fig. 6 Contour map of phreatic groundwater levels simulated by the steady-state model

**Influence of parameter uncertainty on model results**

The adjustment of  $K$  is directly reflected in the gradient of the water table due to Darcy’s law.  $S_y$  represents the capacity of a phreatic aquifer to store or release water, so this parameter impacts the fluctuation of the groundwater level curve.  $K$  and  $S_y$  are both associated with the variation in groundwater levels, which is the fitting target in the calibration process.

**Table 3** Water budget calculated by the transient model and the prediction model (unit:  $\times 10^8 \text{ m}^3/\text{a}$ )

Terms of water budget	2017/ 2018 <sup>a</sup>	Scenario 3 <sup>b</sup>
<b>Recharge items</b>		
River	3.01	2.66
Ephemeral stream	1.88	0
Precipitation	0.43	0.35
Lateral flow	0.08	0.08
Total IN	5.40	3.09
<b>Discharge items</b>		
Wetlands	4.22	3.13
Lakes	0.21	0.21
Total OUT	4.43	3.33
Groundwater storage increase (+)/release (-)	+0.97	-0.24

<sup>a</sup> Values of the water budget in 2017/2018 are the averaged values from 2017 to 2018 calculated by the transient model

<sup>b</sup> Values of the water budget in Scenario 3 are the values from the last year of scenario 3 calculated by the prediction model

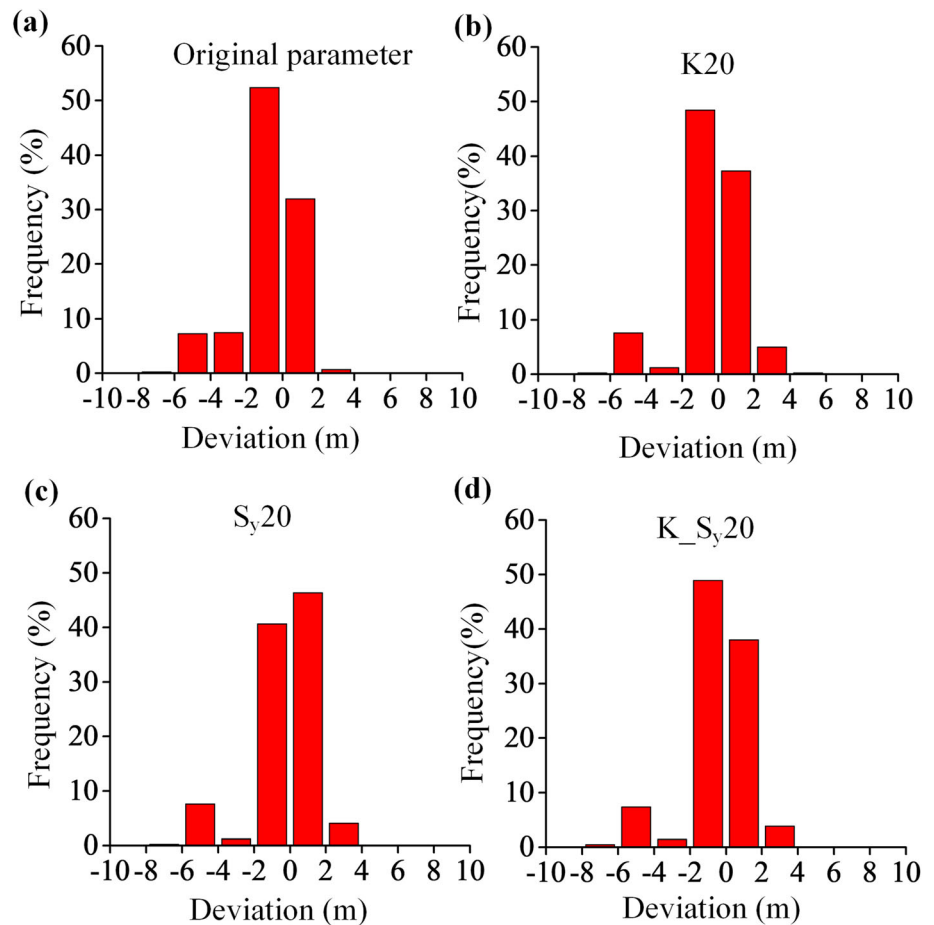
Thus, the two parameters are varied to assess the uncertainty of adapted parameters on the simulation results.

The original calibrated parameters were changed three times, respectively:  $K$  increased by 20% (Fig. 7b),  $S_y$  increased by 20% (Fig. 7c), and  $K$  and  $S_y$  are both increased by 20% (Fig. 7d). When adopting original calibrated parameters, the percentage of the deviation within the interval of  $[-2 \text{ m}, 2 \text{ m}]$  is 85.95% (Fig. 7a). In  $K_{20}$ ,  $S_{y20}$  and  $K_{20} S_{y20}$  (Fig. 7b–d), the proportions of the results within that error interval are 85.75, 86.94 and 86.94%, respectively. The proportion of results with an absolute error greater than 4 m slightly increased from 7.03 to 8.08% ( $K_{20}$ ), 7.84% ( $S_{y20}$ ) and 7.83% ( $K_{20} S_{y20}$ ), respectively. The results show that the error after parameters variation did not expand dramatically, and most of these values changed in the range of  $-2$  to  $2 \text{ m}$ . Drilling was first carried out in low-elevation areas; there are relatively more observations in this area. Groundwater levels in these areas fluctuate little, and they are not sensitive to  $K$  and  $S_y$ . Other factors such as model structure, setting of source and sink, and initial flow field, might be more decisive for the simulation accuracy.

**Model application and discussion**

As mentioned in the preceding, the SLB was chosen as a potential water resource export area in the long-term scheme of water management. To analyze the influence of the water transfer project, the calibrated model was used to simulate the response of groundwater levels to the change in river runoff.

**Fig. 7** The distribution of deviation between simulations and observations. **a** Model results with the calibrated parameters; **b** the model results with  $K$  increased by 20%; **c** the model results with  $S_y$  increased by 20%; **d** the model results with  $K$  and  $S_y$  both increased by 20%



Furthermore, the ecological impacts are discussed based on the prediction of groundwater level decline.

### Scenario settings

In consideration of the water demand (Jiao 2010), four diversion scenarios (1–4, Table 4) were designed to divert river water in the high flow period (July–September). Water will be diverted from the GHR river gauge and stored in the Dang River Reservoir (Fig. 1a).

Considering the increase trend of GHR due to climate change is currently uncertain, conservative historical mean rainfall (Fig. 2) and runoff are applied to the model. The volumes of transfer water are  $0.60 \times 10^8$ ,  $0.80 \times 10^8$ ,  $1.00 \times 10^8$ , and  $1.20 \times 10^8$  m<sup>3</sup>/a, respectively. The residual river flow in scenarios 3 and 4 is close to the base flow, so seasonal streams do not exist in the model in both scenarios. The calibrated parameters ( $K$  and  $S_y$ ) are applied to the prediction model. The time period for the model prediction is 100 years.

**Table 4** The model prediction under four scenarios, with different transfer scales (TS,  $10^4$  m<sup>3</sup>/a). Decline in groundwater level of five observation wells and the flow decline of the Middle Spring

Observation site		Diversion scenario			
		1 (TS 6000)	2 (TS 8000)	3 (TS 10,000)	4 (TS 12,000)
Groundwater level change (m)					
Upstream zone	S01	-15.10	-16.97	-18.60	-20.23
	S02	-1.72	-1.89	-2.07	-2.24
Gobi zone	S05	-14.90	-16.72	-18.69	-21.00
	S06	-6.07	-6.73	-7.46	-8.40
	S11	-4.01	-4.54	-5.10	-5.71
Middle Spring flow change ( $10^4$ m <sup>3</sup> /a)		-1968	-2122	-2325	-2525

## Changes in groundwater levels in the basin

Representative observation wells are selected to analyze the changes in groundwater levels. Water diversion has a significant impact on groundwater levels in the upstream and Gobi zone (Fig. 8). The drawdown of S01 is 15.10 to 20.23 m, which is observed in different conditions (Table 4). However, the drawdown decreases westward on the alluvial fan (Table 4, S02) until it is negligible at the Middle Spring. The results reveal a trend in the upstream region. Specifically, the closer the site is to the river, the more affected the well will be. This finding is also reflected in the Gobi zone. The difference between the predicted and initial groundwater level decreases gradually from east to west (Table 4, S05 to S06 and S11). The maximum drawdown in the valley of the GHR is 51 m in scenario 1 and up to 68 m in scene 4. In contrast, the water-table elevation is reduced by less than 5 m on the north and south side of the SLB. The reason for these differences is that the underlying aquifer of the mountainous area is mainly composed of boulder clay gravel with poor permeability and storage capacity. After 100 years, the groundwater levels in these areas continue to decline until the model reaches an equilibrium state, whereas groundwater levels in the western wetland have stabilized. The groundwater level in the west side of the wetland and Algin Mountain is not affected by water diversion activities, because the groundwater in these places is mainly recharged by rainfall instead of river leakage. In conclusion, except the western part of the basin, the

groundwater drawdown increases with the scale of water division and is influenced by the distance to the river and the physical properties of the aquifer.

## Changes in the relation between groundwater and surface water

Although the groundwater level decline around the Middle Spring is relatively small, the Middle Spring flow obviously decreases over 100 years as the hydraulic gradient continually decreases. The Middle Spring flow decreased from  $1.01 \times 10^8 \text{ m}^3/\text{a}$  to  $0.75\text{--}0.81 \times 10^8 \text{ m}^3/\text{a}$  in 100 years (Table 4). If the prediction model reaches a new balance (when the groundwater storage release = 0), the spring flows will be  $0.40 \times 10^8$ ,  $0.33 \times 10^8$ ,  $0.27 \times 10^8$  and  $0.20 \times 10^8 \text{ m}^3/\text{a}$  in scenarios 1, 2, 3, and 4, respectively. The spring flow only accounted for 40–20% of the initial value. There is a high risk that the Middle Spring will dry up if the project is implemented because it strongly affects the relationship between the groundwater and surface water. The wetland around the Middle Spring will shrink as the ecosystem is maintained by the shallow groundwater and spring water, especially in the dry season. In addition, the seasonal stream decreases dramatically when river water is drawn in the rainy season. In scenario 3 (Table 3, scenario 3), the river leakage is reduced to  $2.66 \times 10^8 \text{ m}^3/\text{a}$ , and the seasonal stream disappears. Discharge in the wetland is reduced to  $3.13 \times$

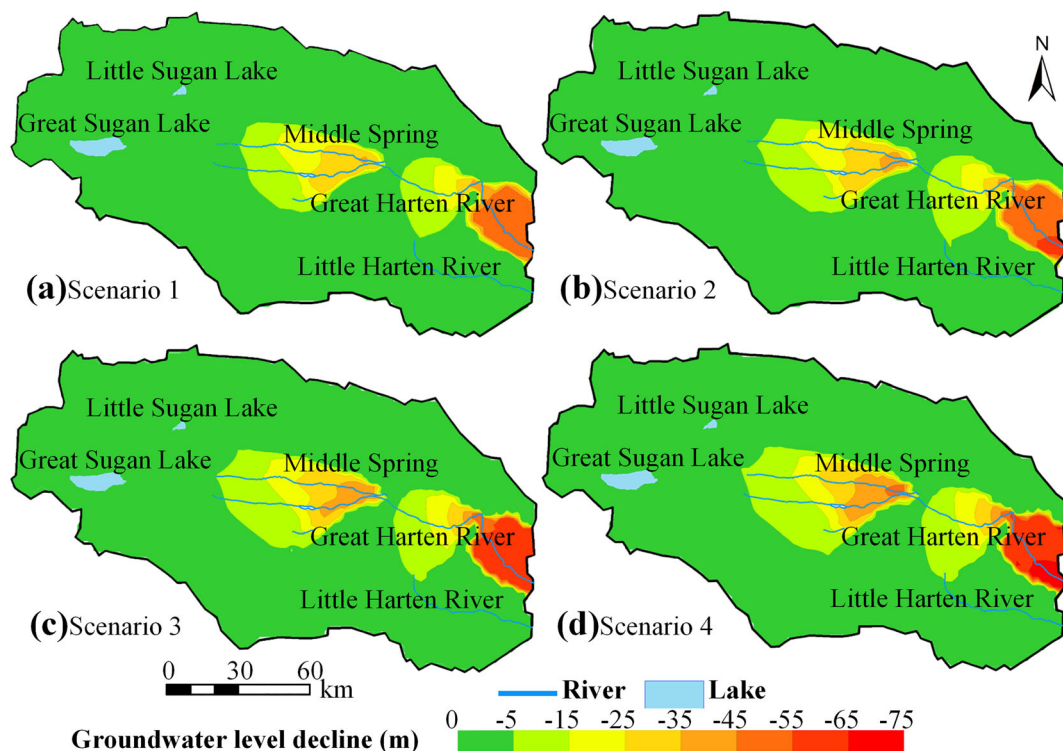


**Fig. 8** a–d Groundwater-level decline of the Suga Lake Basin in the different scenarios compared to the initial water level

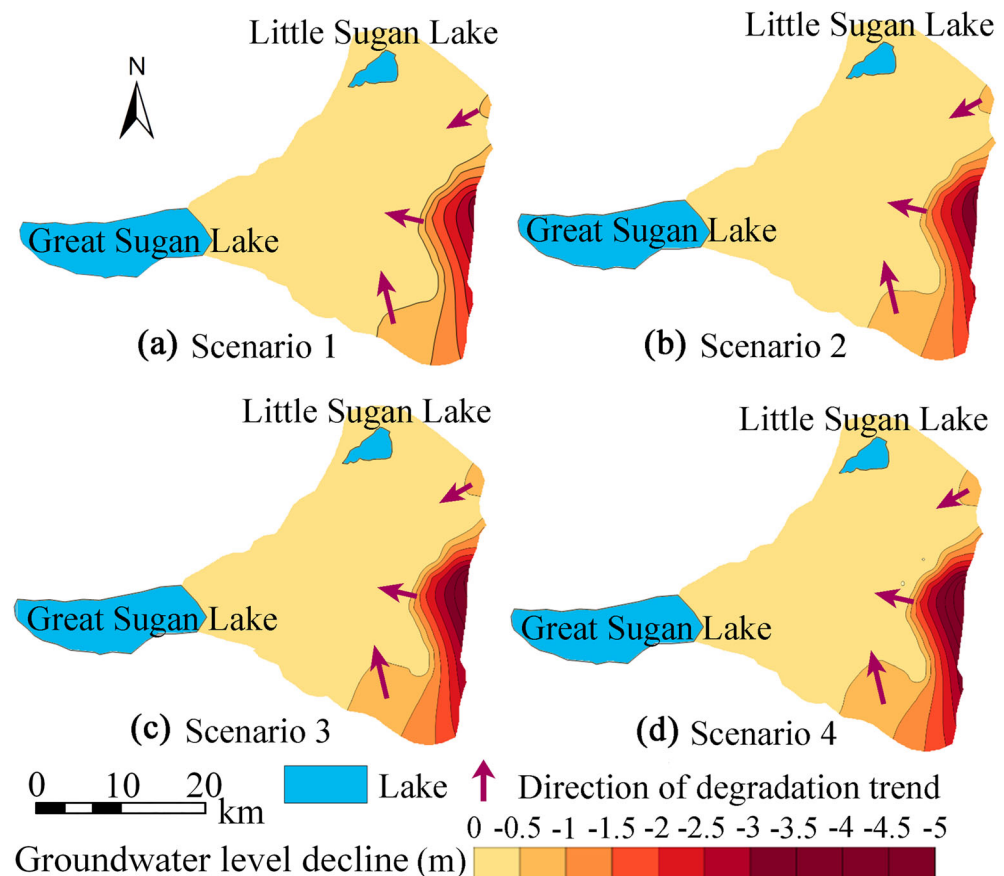
$10^8 \text{ m}^3/\text{a}$  given the decrease in the hydraulic gradient. The reduction of the discharge to lakes is minimal (less than 3%). The diversion has the least effect on the endpoint given the low permeability of the lakebed sediment and low hydraulic gradient. Total discharge is greater than the total recharge with a storage shrinkage rate of  $-0.24 \text{ m}^3/\text{a}$ . The negative balance suggests that the decrease in river infiltration will stimulate the release of storage in the high-elevation aquifer to the central part of the basin.

### Discussion of the influences of the water transfer project on wetlands

The model prediction shows that the groundwater levels at the western wetland decrease (Fig. 9) in any designed cases. The influence of water transfer on the wetland is mainly concentrated in the eastern area rather than the central core area, where the water table changes are less than 0.5 m. Under scenario 1, the largest water level decline in the eastern part of wetland is 3.33 m, which is increased to 4.77 m under scenario 4. The runoff decrease prevents the channel of ephemeral streams from extending to the wetland area (ephemeral stream in Fig. 1c), leading to the groundwater levels decline in the northeast and southeast of the west wetland.

There are two wetlands types in the eastern part of the wetland (Li et al. 2018). The first type is herbaceous swamp, of which the dominant vegetation is *Phragmites communis*, with a coverage of 30–100%. The other type is saline meadow, of which the dominant vegetation is *Kalidium graciale*, with a coverage of 10–30%. Groundwater levels are critical to wetland vegetation and oasis ecology in the arid region of northwest China (Liu et al. 2018; Zhu et al. 2018). *P. communis* grows in areas where the groundwater depth is less than 3 m, and does not tolerate high salinity. *K. graciale*'s roots can reach the maximum depth of 4 m and grow in the soil with severe salinization. Therefore, if the groundwater levels decrease to more than 4 m, the dominant vegetation in the eastern area of wetland will be reduced or even degraded. According to the simulation results of scenario 4 (Fig. 9d), the area with a water level decrease of greater than 4 m is  $10.21 \text{ km}^2$ , accounting for 1.2% of the total wetland area. The groundwater depth in the eastern section is deeper than other areas, so the original vegetation coverage there is the lowest. As a result, the transfer project may cause a decisive impact on the eastern area but less damage to the entire wetland. Vegetation succession will co-occur, transforming the reed into drought-tolerant species. However, ecological consequences caused by

**Fig. 9** a-d The groundwater-level decline of the western wetland in the different scenarios compared to the initial water table



changes in groundwater levels, phreatic-groundwater salinity increase and soil salinity increase, require further assessment based on the relationship between groundwater and vegetation.

## Conclusions

This report describes the modeling of the Sugan Lake Basin, estimating the influence of the interbasin water-transfer project on groundwater levels, springs and wetland vegetation under four transfer scales. The understanding of groundwater system of the Sugan Lake Basin is much improved. The groundwater model is established using FEFLOW software and calibrated for the period of 2016 to 2018. The simulated water table and water budget are consistent with the observed results, suggesting that the groundwater model can reproduce the groundwater system in this pristine basin. The prediction results of the model after 100 years with  $0.6 \times 10^8$ ,  $0.8 \times 10^8$ ,  $1.0 \times 10^8$  and  $1.2 \times 10^8$  m<sup>3</sup>/a transfer scale are analyzed. The main conclusions from the results of this research are as follows:

- The groundwater regimes of the upstream, Gobi and lake zones are different. Dynamic changes in groundwater levels in the Gobi Desert and upstream zone are mainly affected by the surface runoff. Increased river flow significantly increased groundwater levels, particularly in the northern basin. The water level of the two wetlands is dominated by freeze–thaw processes and evapotranspiration.
- The model prediction shows that the groundwater levels in the upstream zone were reduced by maximum 51.10, 56.70, 62.34, and 68.02 m, respectively. The reduction of the Middle Spring flow ranges from  $0.20 \times 10^8$  to  $0.25 \times 10^8$  m<sup>3</sup>/a.
- The smallest water-table decreases are noted in the wetland (less than 5 m), but complex consequences on ecology are caused by these decreases. The project will produce a more significant impact on vegetation coverage in the eastern section of wetland, and natural vegetation succession will occur to some degree.

This present study only focused on fundamental investigation and modeling. Since there is only one river gauge in the basin, the data on flow variation in the middle and lower reaches are not well confined, which leads to simplification of the river in the model. The boreholes do not completely penetrate the water-bearing strata. Thus, the lower confining bed is artificially set, and the model calibration is mainly based on the observed data in the phreatic aquifer. Furthermore, the influences of climate changes are not fully evaluated in this study. The results of the study will provide a basis for future research on wetland ecology and water management in the Sugan Lake Basin.

**Supplementary Information** The online version contains supplementary material available at <https://doi.org/10.1007/s10040-021-02337-9>.

**Acknowledgements** We thank the Institute of Geo-Environmental Monitoring in Gansu Province of China, the Dang River Water Resources Management Bureau in Jiuquan City of Gansu Province of China, and the Tsinghua University for their help and support for fundamental data.

**Funding** This work was supported by the National Natural Science Foundation of China (Grant nos. 41877173 and 41831283) and Beijing Advanced Innovation Program for Land Surface Science.

## References

- Ahmadi A, Zolfaghari MA, Afzali AA (2019) Stability analysis of stakeholders' cooperation in Inter-Basin water transfer projects: a case study. *Water Resour Manag* 33(1):1–18. <https://doi.org/10.1007/s11269-018-2065-7>
- Bao X, Zhang L, Liu N, Song S, Zhao W (2007) Seasonal survey on birds at Suganhu Lake wetland. *Chin J Zool* 42(6):131–135. <https://doi.org/10.13859/j.c>
- Bhaduri A, Barbier E (2011) Water allocation between states in inter-basin water transfer in India. *Intl J River Basin Manag* 9(2):117–127. <https://doi.org/10.1080/15715124.2011.607823>
- Bourblanc M, Blanchon D (2014) The challenges of rescaling South African water resources management: catchment management agencies and interbasin transfers. *J Hydrol* 519:2381–2391. <https://doi.org/10.1016/j.jhydrol.2013.08.001>
- Deepak D (2006) Environmental impact of inter-basin water transfer projects: some evidence from Canada. *Econ Polit Wkly* 41(17):1703–1707. <https://doi.org/10.2307/4418149>
- Diersch HJ (2014) FEFLOW: finite element modeling of flow, mass and heat transport in porous and fractured media. Springer, Heidelberg, Germany. <https://doi.org/10.1007/978-3-642-38739-5>
- Doherty J (2010) PEST: model-independent parameter estimation, user manual, 5th edn. Watermark, Brisbane, Australia
- Fan J, Yang G, Lu H (2016) Study on burial history and Mesozoic hydrocarbon accumulation of Sugan Lake depression on the northern margin of Qaidam Basin. In: Geo-informatics in resource management and sustainable ecosystem. Springer, Heidelberg, Germany. [https://doi.org/10.1007/978-3-662-49155-3\\_101](https://doi.org/10.1007/978-3-662-49155-3_101)
- Feng S, Huo Z, Kang S, Tang Z, Wang F (2011) Groundwater simulation using a numerical model under different water resources management scenarios in an arid region of China. *Environ Earth Sci* 62(5):961–971. <https://doi.org/10.1007/s12665-010-0581-8>
- Gohari A, Eslamian S, Mirchi A, Abedi-Koupaei J, Massah BA, Madani K (2013) Water transfer as a solution to water shortage: a fix that can backfire. *J Hydrol* 491(1):23–39. <https://doi.org/10.1016/j.jhydrol.2013.03.021>
- House AR, Thomson JR, Sorensen JPR, Roberts C, Acreman MC (2015) Modelling groundwater/surface water interaction in a managed riparian chalk valley wetland. *Hydrol Proced* 30:447–462. <https://doi.org/10.1002/hyp.10625>
- Howe CW, Lazo JK, Weber KR (1990) The economic impacts of agriculture-to-urban water transfers on the area of origin: a case study of the Arkansas River Valley in Colorado. *Am J Agric Econ* 72(5):1200–1204. <https://doi.org/10.2307/1242532>
- Hruska T, Toledo D, Sierra CR, Solis GV (2017) Social–ecological dynamics of change and restoration attempts in the Chihuahuan Desert grasslands of Janos Biosphere Reserve, Mexico. *Plant Ecol* 218(1):67–80. <https://doi.org/10.1007/s11258-016-0692-8>

- Hu LT, Jiao JJ (2015) Calibration of a large-scale groundwater flow model using GRACE data: a case study in the Qaidam Basin, China. *Hydrogeol J* 23(7):1305–1317. <https://doi.org/10.1007/s10040-015-1278-6>
- Huang J, Yu H, Guan X, Wang G, Guo R (2015) Accelerated dryland expansion under climate change. *Nat Clim Chang* 6(2):166–171. <https://doi.org/10.1038/nclimate2837>
- Jasinski MF, Stoll JD, Hancock D, Robbins J, et al. (2020) ATLAS/ICESat-2 L3A inland water surface height, version 3. Boulder, Colorado USA. NASA National Snow and Ice Data Center distributed active archive center. <https://doi.org/10.5067/ATLAS/ATL13.003>
- Jiao JJ (2010) Crescent moon spring: a disappearing natural wonder in the Gobi Desert, China. *Groundwater* 48(1):159–163. <https://doi.org/10.1111/j.1745-6584.2009.00599.x>
- Jolly ID, McEwan KL, Holland KL (2008) A review of groundwater–surface water interactions in arid/semiarid wetlands and the consequences of salinity for wetland ecology. *Ecohydrol* 1(1):43–58. <https://doi.org/10.1002/eco.6>
- Kingsford RT, Thomas RF (2004) Destruction of wetlands and waterbird populations by dams and irrigation on the Murrumbidgee River in arid Australia. *Environ Manag* 34(3):383–396. <https://doi.org/10.1007/s00267-004-0250-3>
- Li B, Chen Y, Chen Z, Li W (2012) Trends in runoff versus climate change in typical rivers in the arid region of Northwest China. *Quat Int* 282:87–95. <https://doi.org/10.1016/j.quaint.2012.06.005>
- Li Y, Liu K, Gao Y MQ, Wang M (2018) Influence of the Yinhajidang project on the natural vegetation in Sugan Lake wetland. *Adm Tech Environ Monit* 30(02):61–64
- Lin J, Ma R, Hu Y, Sun Z, Wang Y, McCarter CPR (2018) Groundwater sustainability and groundwater/surface-water interaction in arid Dunhuang Basin, Northwest China. *Hydrogeol J* 26(5):1559–1572. <https://doi.org/10.1007/s10040-018-1743-0>
- Liu C, Zheng H (2002) South-to-north water transfer schemes for China. *Int J Water Resour Dev* 18(3):453–471. <https://doi.org/10.1080/079006202200006934>
- Liu M, Jiang Y, Xu X, Huang Q, Huo Z, Huang G (2018) Long-term groundwater dynamics affected by intense agricultural activities in oasis areas of arid inland river basins, Northwest China. *Agric Water Manag* 203:37–52. <https://doi.org/10.1016/j.agwat.2018.02.028>
- Luo PP, Sun YT, Wang ST, Wang SM, Lyu JQ, Zhou MM, Nakagami K, Takara K, Nover D (2020) Historical assessment and future sustainability challenges of Egyptian water resources management. *J Clean Prod* 263(1):1–11. <https://doi.org/10.1016/j.jclepro.2020.121154>
- Lyu JQ, Luo PP, Mo SH, Zhou MM, Shen B, Nover D (2019) A quantitative assessment of hydrological responses to climate change and human activities at spatiotemporal within a typical catchment on the Loess Plateau, China. *Quat Int* 527:1–11. <https://doi.org/10.1016/j.quaint.2019.03.027>
- Ma J, He J, Qi S, Zhu G, Zhao W, Edmunds WM, Zhao Y (2013) Groundwater recharge and evolution in the Dunhuang Basin, northwestern China. *Appl Geochem* 28(28):19–31. <https://doi.org/10.1016/j.apgeochem.2012.10.007>
- Ma Z, Wang Z, Gu Y, Xia T (2015) Ecological vulnerability assessment of nature reserve in arid region of Northwest China: a case study of the Xihu Nature Reserve and the Suganhu Nature Reserve in Gansu. *J Desert Res* 35(1):253–269. <https://doi.org/10.7522/j.issn.1000-694X.2014.00153>
- Mohammed R, Scholz M (2018) Climate change and anthropogenic intervention impact on the hydrologic anomalies in a semiarid area: lower Zab River basin, Iraq. *Environ Earth Sci* 77(10):357. <https://doi.org/10.1007/s12665-018-7537-9>
- Reynolds JF, Smith DMS, Lambin EF, Turner BL et al (2007) Global desertification: building a science for dryland development. *Science* 316(5826):847–851. <https://doi.org/10.1126/science.1131634>
- Rivière A, Gonçalves J, Jost A, Font M (2014) Experimental and numerical assessment of transient stream–aquifer exchange during disconnection. *J Hydrol* 517:574–583. <https://doi.org/10.1016/j.jhydrol.2014.05.040>
- Rodrigues D, Gupta H, Serrat-Capdevila A, Oliveira PT, Mendiondo E, Iii T, Mahmoud M (2014) Contrasting American and Brazilian systems for water allocation and transfers. *J Water Resour Plan Manag* 141(7):1–11. [https://doi.org/10.1061/\(ASCE\)WR.1943-5452.0000483](https://doi.org/10.1061/(ASCE)WR.1943-5452.0000483)
- Roy PK, Roy SS, Giri A, Banerjee G, Majumder A, Mazumdar A (2015) Study of impact on surface water and groundwater around flow fields due to changes in river stage using groundwater modeling system. *Clean Techn Environ Pol* 17(1):145–154. <https://doi.org/10.1007/s10098-014-0769-9>
- Scanlon BR, Keese KE, Flint AL, Flint LE, Gaye CB, Edmunds WM, Simmers I (2010) Global synthesis of groundwater recharge in semi-arid and arid regions. *Hydrol Process* 20(15):3335–3370. <https://doi.org/10.1002/hyp.6335>
- Shi Y, Shen Y, Kang E, Li D, Ding Y, Zhang G, Hu R (2006) Recent and future climate change in Northwest China. *Clim Chang* 80(3–4):379–393. <https://doi.org/10.1007/s10584-006-9121-7>
- Tian Y, Zheng Y, Wu B, Wu X, Liu J, Zheng C (2015) Modeling surface water–groundwater interaction in arid and semiarid regions with intensive agriculture. *Environ Model Softw* 63:170–184. <https://doi.org/10.1016/j.envsoft.2014.10.011>
- Tien BD, Talebpour Asl D, Ghanavati E, Al-Ansari N, Khezri S, Chapi K, Amini A, Thai Pham B (2020) Effects of Inter-Basin water transfer on water flow condition of Destination Basin. *Sustainability* 12(1):338. <https://doi.org/10.3390/su12010338>
- USGS (2020) EarthExplorer. <https://earthexplorer.usgs.gov/>. Accessed January 2020
- Vrzal L, Vižintin Ogrinc R (2019) An integrated approach for studying the hydrology of the Ljubljansko Polje aquifer in Slovenia and its simulation. *Water* 11:1753. <https://doi.org/10.3390/w11091753>
- Wang G, Gong T, Lu J, Lou D, Hagan DFT, Chen T (2018) On the long-term changes of drought over China (1948–2012) from different methods of potential evapotranspiration estimations. *Int J Climatol* 38(7):2954–2966. <https://doi.org/10.1002/joc.5475>
- Xiang J, Zhou JJ, Yang JC, Huang MH et al (2020) Applying multivariate statistics for identification of groundwater chemistry and qualities in the Sugan Lake Basin, northern Qinghai-Tibet plateau, China. *J Mt Sci* 17(2):448–463. <https://doi.org/10.1007/s11629-019-5660-z>
- Yao Y, Zheng C, Liu J, Cao G, Xiao H, Li H, Li W (2015) Conceptual and numerical models for groundwater flow in an arid inland river basin. *Hydrol Process* 29(6):1480–1492. <https://doi.org/10.1002/hyp.10276>
- Zhang K, An Z, Cai D, Guo Z, Xiao J (2016) Key role of desert-oasis transitional area in avoiding oasis land degradation from Aeolian desertification in Dunhuang, Northwest China. *Land Degrad Dev* 28(1):142–150. <https://doi.org/10.1002/ldr.2584>
- Zhang M, Hu L, Yao L, Yin W (2018) Numerical studies on the influences of the south-to-north water transfer project on groundwater level changes in the Beijing plain, China. *Hydrol Process* 32(12):1858–1873. <https://doi.org/10.1002/hyp.13125>

- Zhou D, Wang X, Shi M (2016) Human driving forces of oasis expansion in northwestern China during the last decade: a case study of the Heihe River basin. *Land Degrad Dev* 28(2):412–420. <https://doi.org/10.1002/ldr.2563>
- Zhu X, Wu J, Nie H, Guo F, Wu J et al (2018) Quantitative assessment of the impact of an inter-basin surface-water transfer project on the groundwater flow and groundwater-dependent eco-environment in an oasis in arid northwestern China. *Hydrogeol J* 26(5):1475–1485. <https://doi.org/10.1007/s10040-018-1804-4>

**Publisher's note** Springer Nature remains neutral with regard to jurisdictional claims in published maps and institutional affiliations.